Electron Transfer Reactivity of $O_2 + O_2^-$ System in Low-Spin Coupling: *Ab Initio* Study at Electron Correlation Level

YUXIANG BU,[1,2] HAITAO SUN,[2] HONGBO NIU[3]

[1] *Institute of Theoretical Chemistry, Shandong University, Jinan 250100, People's Republic of China*
[2] *Department of Chemistry, Qufu Normal University, Qufu 273165, People's Republic of China*
[3] *Department of Chemistry, Yantai Education College, Yantai 264000, People's Republic of China*

Received 25 September 1998; accepted 19 January 1999

ABSTRACT: The electron transfer reactivity of the $O_2 + O_2^-$ system in low-spin coupling is studied at the second-order unrestricted Møller–Plesset (full)/6-311 + G* basis set level by using different transition state structures. The properties and stabilities of the encounter complexes are compared for the five selected coupling structures: two *T* type, collinear, parallel, and crossing. The activation barriers and the coupling matrix elements are also calculated. The results indicate that the structures of the encounter complexes directly affect the electron transfer mechanism and rate. These encounter complexes are structurally unstable, the contact distances between the acceptor O_2 and the donor O_2^- are generally large, the interaction is weak, and the structures are floppy. The electronic transmission factor for the reacting system, $O_2 + O_2^-$, is less than unity; thus, the electron transfer reaction is nonadiabatic in nature. Analysis of the dependence of relevant kinetic parameters on various influencing factors has shown that the effect of the solvent medium on the coupling matrix element is small but that on the electron transfer rate is very large. Among the five selected transition state structures, the electron transfer is more likely to take place via T_1-type and *P*-type structures. In the low-spin coupling the favorable electronic states for two reacting species are $^1\Sigma_g^+(O_2)$ and $X^2\Pi_g(O_2^-)$ instead of $X^3\Sigma_g^-(O_2)$ and $X^2\pi_g(O_2^-)$, which are favorable for the high-spin (quartet state) coupling mechanism. © 1999 John Wiley & Sons, Inc. J Comput Chem 20: 989–998, 1999

Keywords: electron transfer reactivity; encounter complex; *ab initio* calculation analysis; $O_2 + O_2^-$ system in low-spin coupling

Correspondence to: Y. Bu; e-mail: buyux@ji-public.sd.cninfo.net

Contract/grant sponsors: Natural Science Foundation of Shandong Province; National Natural Science Foundation of China

© 1999 John Wiley & Sons, Inc.
CCC 0192-8651 / 99 / 100989-10

Introduction

The simple electron transfer reaction theory provided by various researchers[1–5] has been demonstrated as a useful tool in rationalizing the structure dependence of the electron transfer reactivity. Now it has been extensively applied to approach various charge transfer processes. In this theory the electron transfer reaction nominally contains five elementary stages: formation of the precursor complex, reorganization and activation of the precursor complex, electron transfer, relaxation of the successor complex, and dissociation of the successor complex. For the following thermal electron self-exchange reaction between the acceptor O_2 and the donor O_2^- depicted by eq. (1), these elementary stages may be expressed by eqs. (2)–(6).

$$O_2(r_a) + O_2^-(r_b) = O_2^-(r_b) + O_2(r_a), \quad (1)$$

$$O_2(r_a) + O_2^-(r_b) = O_2(r_a)\cdots O_2^-(r_b), \quad (2)$$

$$O_2(r_a)\cdots O_2^-(r_b) = O_2(r_a^*)\cdots O_2^-(r_b^*), \quad (3)$$

$$O_2(r_a^*)\cdots O_2^-(r_b^*) = O_2^-(r_a^*)\cdots O_2(r_b^*), \quad (4)$$

$$O_2^-(r_a^*)\cdots O_2(r_b^*) = O_2^-(r_b)\cdots O_2(r_a), \quad (5)$$

$$O_2^-(r_b)\cdots O_2(r_a) = O_2^-(r_b) + O_2(r_a), \quad (6)$$

Obviously, eq. (2) is the preequilibrium equation and its energy change corresponds to the sum of the electrostatic work required to bring together the reactants and the stabilization energy. The products in eq. (2) are the encounter complex, and they may be in various different structural forms. The energy change in eq. (3) corresponds to the activation energy.

Provided that the elementary electron transfer step is rate determining, the overall observed rate constants of outer sphere electron transfer reactions, k_{obsd}, can be expressed as[6]

$$k_{obsd} = K_p k_{et} \quad (7)$$

where K_p is the equilibrium constant for forming the precursor state (the encounter complex) from the separated reactants and k_{et} is the unimolecular rate constant for the electron transfer step. In general, it is convenient to consider an electrostatic work-corrected rate constant, k_{cor}, that would equal k_{obsd} in the absence of Coulombic work terms.

$$k_{cor} = K_o k_{et}^{cor} \quad (8)$$

where K_o and k_{et}^{cor} are work-corrected values of K_p and k_{et}, respectively. The quantity k_{et}^{cor} can be related to the work-corrected free energy of activation, ΔG^*, by[5]

$$k_{et}^{cor} = \nu_n \Gamma_n \kappa_{el} \exp(-\Delta G^*/RT). \quad (9)$$

Obviously, for the title reaction, because the oxidized species O_2 in the reactants is uncharged and the reduced species O_2^- is only charged by a small value (-1), the electrostatic-Coulombic work term is very small. The electron transfer rate may actually be expressed as

$$k_{obsd} = K_p \nu_n \Gamma_n \kappa_{el} \exp(-\Delta G^*/RT), \quad (10)$$

where ν_n is a nuclear frequency factor (per second), Γ_n is a nuclear tunneling factor, and κ_{el} is an electronic transmission coefficient. Equation (10) provides an association of the experimental electron transfer rate with the electron transmission factor, the Franck–Condon barrier, ΔG^*, and the other quantities that are of central significance in electron transfer theory.

The electronic transmission coefficient refers primarily to the electronic coupling interaction between the initial state and the final state of the reactants, and it denotes the adiabaticity or the nonadiabaticity of the electron transfer reaction. From the Landau–Zener (LZ) principle, the electronic transmission coefficient can be expressed as

$$\kappa_{el} = 2P_0/(1 + P_0), \quad (11a)$$

where P_0 is the probability for hopping from the initial to the final diabatic potential energy surfaces on a single passage of the system through the region; it may be obtained by

$$P_0 = 1 - \exp\left(-4\pi^2 H_{if}^2/(h\nu_s|S_2 - S_1|)\right), \quad (11b)$$

where h is the Planck constant, v_s is the velocity (assumed constant) with which the reacting system passes through the intercross region along the reaction coordinate, $|S_2 - S_1|$ is the slope difference of the potential energy surfaces of the initial and the final states at the transition state, and H_{if} is the matrix element coupling the two electronic states (the reactants and the products). The accurate determination of this factor is very important in calculating the correct electron transfer rate.

An assumption that the transmission coefficient is equal to unity is usually used in general calculations of the rate constant or the activation energy. Obviously this assumption is not reasonable for

many electron transfer reactions. Many studies were done to calculate the coupling matrix element and electronic transmission coefficient in terms of LZ formalism for the electron transfer reaction involving some transition metal ions in solution.[4,5,7–9] However, many of them adopted some approximations in which the original LZ formula was reduced into a simple formalism and the electronic transmission coefficient was evaluated from the activation energy.

Another main factor influencing the electron transfer rate is the activation energy. In the calculation of the activation barrier, an approximate method is usually used to separate ΔG^* into additive contributions arising from the (inner sphere) distortions of the reacting species and the (outer sphere) reorientation of the surrounding solvent. In developing accurate treatment schemes for this energy quantity, great progress has been made; a considerable amount of theoretical work has been devoted to the development of models.[10–15] However, these models have only been used to calculate the activation energy in terms of the potential energy surfaces of the isolated species; no attempt has been made to directly calculate the energy quantity in terms of the potential energy surfaces of the coupled reacting system.

Obviously, the determinations of these quantities strongly depend on the potential energy surface of the reacting system and further on the structure and properties of the encounter complex and the activated complex. However, the encounter or the activated complexes are unstable and are not easily amenable to experimental observation; thus, detailed interpretation of the electron transfer rate and mechanism in terms of relevant experimental data becomes very difficult. In the absence of available experimental data, *ab initio* calculation has played an auxiliary role in providing relevant information and in helping to elucidate the fundamental aspects regarding this encounter complex and its structure reorganization in the activation process. In some respects this electron transfer encounter complex provides more of a challenge to the theoreticians and the experimentalists than the stable molecules and other reacting intermediate species. The presence of this anion encounter complex necessitates the use of a more flexible basis set than the one used for neutral or charged systems.[16] On the other hand, this donor–acceptor encounter complex is generally in a high-spin state, and its structure and properties are not well described by a simple quantum chemistry method; some high quality treatment of electron correlation is essential for an accurate determination of the potential energy surfaces and relevant activation kinetic parameters. Great progress has been made in well characterizing these systems. In particular, during recent years enormous progress has been made in the experimental study of the interaction in the gas-phase ionic clusters. These studies constitute very important and fundamental sources of information for understanding various structures and spectroscopic properties of the supermolecular complexes and the encounter complex in reaction processes and their affect on the chemical reactivities. Of particular interest are the studies on the interaction between the small functional biological molecules, because these studies may provide some important information concerning the living process mechanism.

Being perhaps the simplest model of the anion encounter complex, $O_2 \cdots O_2^-$ received a great deal of attention from the theoretical standpoint.[17–21] However, early *ab initio* calculations on this system were restricted to rather small basis sets and did not include electron correlation effects.[18] More recent works improved on the basis set used to study the isolated species $[O_2(X^3\Sigma g^-)$ and $O_2^-(X^2\Pi_g)]$ systematically,[16,22] but no attempt was made to study the encounter complex systematically or to understand the nature of the interaction between the donor and the acceptor and the electron transfer reactivity.

The main purpose of the present work was, first, to obtain a more complete understanding of the nature of the interaction in the $O_2 \cdots O_2^-$ complex in the low-spin coupling mechanism (in the doublet state) and, second, to obtain relevant electron transfer kinetic parameters and to compare the effect of the encounter complex structures on these kinetic parameters. Geometry optimization was performed at the self-consistent field (SCF) and the electron correlation levels using a fairly large basis set with two sets of polarization functions. Several possible structures and corresponding energy properties were compared, and a complete set of vibrational frequencies and charge populations were calculated. In the calculation of the electron transfer rate, the activation energies were calculated via a new *ab initio* scheme. The electronic transmission factor was calculated in terms of the LZ two-state model with some *ab initio* calculated quantities (the coupling matrix element and slopes of potential energy surfaces). The results were compared with the corresponding experimental value.

Theoretical Model and Computational Details

SIMPLE DESCRIPTION OF THEORETICAL MODEL

Activation Barrier

At the activated state, the energy of the activated complex $O_2(r_a^*)\cdots O_2^-(r_b^*)$ before electron transfer is expressed as

$$E_i = E_{O_2\cdots O_2^-}(r_a^*, r_b^*). \quad (12)$$

After the electron transfer, the energy of this system becomes

$$E_f = E_{O_2^-\cdots O_2}(r_a^*, r_b^*), \quad (13)$$

where $E_j(r^*)$ denotes the energy of the reacting complex $[O_2 \cdots O_2^-]$ at the activation state, r_a^* is the nuclear configuration of the O_2 molecular fragment, and r_b^* is that of the O_2^- molecular fragment. The energy conservation principle during the transition requires that $E_f = E_i$, thus,

$$E_{O_2\cdots O_2^-}(r_a^*, r_b^*) = E_{O_2^-\cdots O_2}(r_a^*, r_b^*). \quad (14)$$

Because O_2^- and O_2 are two systems with different properties, eq. (14) suggests that r_a^* should be equal to r_b^*. Therefore, the energy of the system $(O_2 \cdots O_2^-)$ at the activated state is given by

$$E_a^* = E_{O_2\cdots O_2^-}(r_a^*, r_a^*). \quad (15)$$

Obviously eq. (15) represents the energy curve formed in the crossing between the two diabatic potential energy surfaces corresponding to the initial and the final states of the electron transfer, respectively. Minimization of eq. (15) gives the some relevant activation parameters.

The adiabatic activation energy (E_a) is then easily obtained by subtracting the energy of each encounter complex from the corresponding energy at the activated state, namely,

$$E_a = E_{O_2\cdots O_2^-}(r_a^*, r_a^*) - E_{O_2\cdots O_2^-}(r_{O_2}, r_{O_2^-}). \quad (16)$$

Similarly, the energy of this system at the crossing point, E_c, is also calculated by using the energy dependence on the O—O distance for both isolated species O_2 and O_2^-, $E_{O_2}(r_a^*)$, and $E_{O_2^-}(r_b^*)$, in eq. (15). The diabatic activation energy (E_d) is then obtained by subtracting the energies of two isolated species (O_2 and O_2^-) at their own equilibrium geometries from E_c.

$$E_d = E_{O_2}(r_a^*) + E_{O_2^-}(r_b^*) - E_{O_2}(r_a) - E_{O_2^-}(r_b). \quad (17)$$

Electronic Coupling Matrix Element

The electronic coupling matrix element actually is the energy lowering caused by the coupling between the initial and the final states of electron transfer; thus, it may be obtained by

$$H_{if} = E_d - E_a. \quad (18)$$

Slopes of Potential Energy Surfaces

For a given potential energy surface, $E(Q)$, the value of its slope, S_j, can be obtained from the relationship

$$S_j = -\partial E_j(Q)/\partial Q, \quad (19)$$

where $E_j(Q)$ is the potential energy surface of the reactant state ($j = 1$) or that of the product state ($j = 2$) as a function of the reaction coordinate, Q. In general, the nuclear configuration of the reacting species in the reactant state or in the product state changes linearly, accompanying the change of the reaction coordinate for the reacting system in proceeding from the initial state to the transition state and then to the final state. Using the 1-dimensional linear reaction coordinate, the differential element of the reaction coordinate, dQ, may relate to that of the molecular nuclear configuration displacement, dq.

$$xdQ = dq \quad (20)$$

where x is the total nuclear configuration change of the corresponding species. Thus, eq. (19) may be rewritten as

$$S_j = -\partial E_j(q)/\partial q, \quad (21)$$

where E_j corresponds to eq. (12) for $j = 1$ or eq. (13) for $j = 2$ as a function of the O—O displacement from the stable encounter complex geometries.

Substituting eqs. (12) and (13) into eq. (21), the slopes of the reactant and the product states may

be obtained by

$$\begin{aligned} S_1 &= -\partial E_i(q_r)/\partial q_r \\ &= -\partial E_{O_2,\ldots,O_2^-}(q_{O_2^-}, q_{O_2})/\partial q_{O_2^-} \\ &\quad + \partial E_{O_2\cdots O_2^-}(x - q_{O_2^-}, q_{O_2})/\partial(x - q_{O_2^-}) \\ &= S_{O_2^-} - S_{O_2}, \end{aligned} \tag{22}$$

$$\begin{aligned} S_2 &= -\partial E_j(q_0)/\partial q_0 \\ &= \partial E_{O_2^-\cdots O_2}(x - q_{O_2}, q_{O_2^-})/\partial(x - q_{O_2}) \\ &\quad - \partial E_{O_2^-\cdots O_2}(q_{O_2}, q_{O_2^-})/\partial q_{O_2} = -S_{O_2^-} + S_{O_2}. \end{aligned} \tag{23}$$

The slope difference between the reactant and the product states may be further expressed as

$$|S_2 - S_1| = 2|S_{O_2^-} - S_{O_2}| \tag{24}$$

where SO_2^- and SO_2 denote the slopes of the potential energy surfaces of the reduced (the donor molecular fragment) and the oxidized (the acceptor molecular fragment) species, respectively, in the activated complex at the transition state.

COMPUTATIONAL DETAILS

Geometrical optimizations and electronic structure calculations were made at the second-order unrestricted Møller–Plesset (MP) perturbation theory level including full-orbital space electron correlation [UMP2 (full)] with the 6-311 + G* basis set. All calculations were carried out using the Gaussian 92 package[23] for the encounter complex (O_2—O_2^-) and relevant isolated species [$O_2(X^3\Sigma_g^-)$, $O_2(^1\Sigma_g^+)$, and $O_2^-(X^2\Pi_g)$]. In calculations of the $O_2\cdots O_2^-$, five selected structures, such as two T types (T_1 and T_2), collinear (L), parallel (P), and crossing (C), were designed and are shown in Figure 1. The former four structures are assumed to be in plane in order to keep the largest overlap between the electron donor orbital, π^* of O_2^-, and the electron acceptor orbital, π^* of O_2.

No problems arose in calculations for the isolated species [$O_2(X^3\Sigma_g^-)$, $O_2(^1\Sigma_g^+)$, and $O_2^-(X^2\Pi_g)$]. For the encounter complex, the five structure forms were optimized under the symmetry constraint with respect to the contact distance and the O—O distances in the fragments O_2 (r_0) and O_2^- (r_-) in the encounter complex (see Fig. 1). The stabilization energy of the corresponding encounter complex may be obtained from the difference between the corresponding encounter complex and the isolated species, $O_2(X^3\Sigma_g^-)$, $O_2(^1\Sigma_g^+)$, and $O_2^-(X^2\Pi_g)$. The transition state is defined as the lowest energy point along this symmetric energy seam, which is obtained from eq. (16). All these energy quantities are calibrated at the UMP4 (full, SDTQ)/6-311 + G* level.

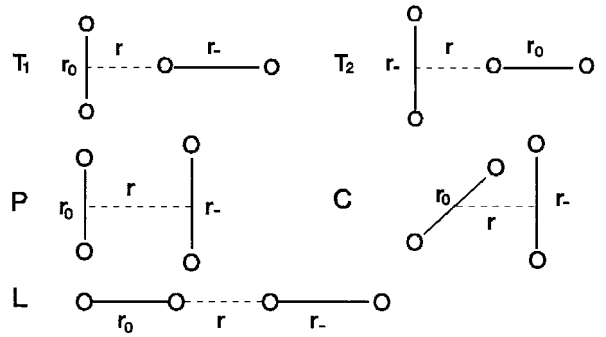

FIGURE 1. The sketch of the five molecular structures for the encounter complex. r_0 and r_- denote the O—O distances in the molecular fragments O_2 and O_2^-, respectively, in the encounter complex and r denotes the contact distance.

In the determination of the potential energy surfaces for every molecular fragment species, the single point calculation method was used at the full-electron correlation level [MP2 (full)/6-311 + G*]. On the basis of the fully optimized geometries, the potential energy curve of the donor molecular fragment can be obtained by fixing the contact distance (r) and the O—O distance in another molecular fragment at the optimized values. Corresponding continuous potential energy curves were obtained by fitting the calculated energy points to an eighth-degree polynomial in r. The data were also fitted to a sixth-degree polynomial as a check for possible error due to the fitting procedure and no substantive changes in the results were observed. The fitted potential energy curve can be expressed as

$$E(r) = a_0 + a_1 r + a_2 r^2 + \cdots + a_7 r^7, \tag{25}$$

and can also be expressed as

$$E(r - r_e) = E(r_e) + \frac{1}{2}k_2(r - r_e)^2 + \frac{1}{6}k_3(r - r_e)^3 + \cdots + \frac{1}{n!}k_n(r - r_e)^n. \tag{26}$$

Results and Discussion

OPTIMIZED STRUCTURES AND PROPERTIES OF ISOLATED SPECIES

Calculations on the isolated species $O_2(X^3\Sigma_g^-)$, $O_2(^1\Sigma_g^+)$, and $O_2^-(X^2\Pi_g)$ were first performed at the UMP2 level including all electron correlation with the 6-311 + G* basis set. The optimized relevant spectroscopic properties are summarized in Table I. By comparing the calculated and experimental values for the spectroscopic constants, some trends in the dependence of the quality of the results on the level of theory can be identified. Good agreement of the calculated values with the experimental findings can be observed for the spectroscopic parameters (r_e, ω_e, B_e, and D_J) in Table I. These quantities were also calculated at the Hartree–Fock (HF) level. A comparison indicates that even if a larger basis set such as 6-311 + G* was used, the calculated HF equilibrium internuclear distances for species $O_2(X^3\Sigma_g^-)$, $O_2(^1\Sigma_g^+)$, and $O_2^-(X^2\Pi_g)$ had larger errors. Inclusion of full electron correlation correction decreased the errors in the internuclear distances, and significant accuracy was achieved at the MP2 (full)/6-311 + G* level with a small error. The calculated results of r_e, ω_e, $\omega_e x_e$, and D_J for the three isolated species $O_2(X^3\Sigma_g^-)$, $O_2(^1\Sigma_g^+)$, and $O_2^-(X^2\Pi_g)$ at this correlation level were also very close to the results obtained using the other correlation method. In addition, the adiabatic ionization energy of the species $O_2^-(X^2\Pi_g)$ was calculated to be 0.38 eV at this theoretical level, which was in reasonable agreement with the experimental value of 0.44 eV.[24] This analysis fully confirmed that this full electron second-order correlation method is applicable in investigating the structures and spectroscopic properties of these small species containing an oxygen element and its relevant molecules.

ENCOUNTER COMPLEXES AND TRANSITION STATE

The encounter complex is an important reaction intermediate in the electron transfer process. Its geometrical configuration directly influences not only the activation energy of the reaction but also the electron transfer coupling matrix element and the electron transfer rate. To test the effect of the encounter complex structure on the electron transfer reactivity, it is very important to find various possible geometrical configurations for the encounter complex. Actually, there are two key orbitals in determining the electronic state for the species O_2 and O_2^-: one is the π^* orbital in plane and another is that out of plane. This set of π^* orbitals accommodates two and three electrons,

TABLE I.
Calculated Spectroscopic Properties for $O_2(X^3\Sigma_g^-)$, $O_2(^1\Sigma_g^+)$, and $O_2^-(X^2\Pi_g)$.

		r_e (Å)	ω_e (cm^{-1})	$\omega_e x_e$ (cm^{-1})	$D_J \times 10^6$ (cm^{-1})	D_e (eV)
$O_2^-(X^2\Pi_g)$	Experiment[a]	1.347	1090.0	−8.1		4.161
	HF / 6-311 + G*	1.285	1176.9	−7.2	4.096	1.235
	MP2 / 6-311 + G*	1.356	1145.3	−7.8	4.711	3.062
	CCSD / aug-cc-pvDZ[b]	1.352	1146.4	−8.22	4.685	3.482
	QCISD / aug-cc-pvDZ[b]	1.353	1127.5	−8.24	4.795	3.495
$O_2(X^3\Sigma_g^-)$	Experiment[a]	1.2075	1580.2	−11.98	4.839	5.213
	HF / 6-311 + G*	1.155	1712.0	−9.82	3.854	1.478
	MP2 / 6-311 + G*	1.222	1635.4	−10.76	4.035	4.125
	CCSD / aug-cc-pvDZ[b]	1.211	1641.0	−11.22	4.421	4.380
	QCISD / aug-cc-pvDZ[b]	1.212	1624.9	−11.47	4.471	4.403
$O_2(^1\Sigma_g^+)$	MP2 / 6-311 + G*	1.247	1563.4			3.733
	MP2 / aug-cc-pvDZ	1.259	1599.6			3.830
	QCISD / 6-311 + G*[c]	1.211	1645.5			2.917
	QCISD / aug-cc-pvDZ[c]	1.220	1674.9			2.955

The all electron correlation is included in MP2, CCSD, and QCISD electron correlation calculations.
[a] From ref. 27.
[b] From ref. 16.
[c] Our calculated data.

respectively. The encounter in plane of O_2 with O_2^- is preferred because the orbital phase symmetry suggests that the overlap between the electron donor orbital, π^* of O_2^-, and the electron acceptor orbital, π^* of O_2, would be the largest when all four oxygen atoms are in a plane. Thus, four coplane geometries were designed (two T shaped T_1 and T_2, linear L, and parallel P) and are shown in Figure 1. A cross nonplane geometrical configuration was also designed (C type, see Fig. 1). For every species the in-plane and the out of plane components of the π^* orbitals are assigned to $\pi_=^*$ and $\pi_\perp^*$ representations, respectively. The two lowest states of O_2 are the $^3\Sigma_g^-$ and $^1\Sigma_g^+$ with the electronic configuration $(\pi_=^*)^1(\pi_\perp^*)^1$ (there are two different spin ways for these two states), and the ground state of O_2^- is the $^2\Pi_g$ state with two possible electronic configurations: $(\pi_=^*)^2(\pi_\perp^*)^1$ and $(\pi_=^*)^1(\pi_\perp^*)^2$. In forming the combined $O_2 \cdots O_2^-$ system, there are two possible spin coupling schemes. The aim of this study was at the low-spin coupling mechanism of electron transfer reactivity, because this process can distinguish the dependence of the electron transfer coupling mechanism on the initial electronic states of the reactant molecules.

Preliminary calculations indicated that the encounter complexes in low-spin coupling from $O_2(^3\Sigma_g^-)$ and $O_2^-(X^2\Pi_g)$ seem to be unfavorable from the energy standpoint, because the stabilization energies for these encounter complexes in the doublet state are calculated to be -10.201 (T_1, $^2B_1$), -9.519 (T_2, $^2A_2$), 0.840 (L, $^2A_2$), -9.833 (P, $^2A_2$), and -9.201 (C, $^2A_1$) kcal/mol relative to the two isolated reactant molecules $O_2(^3\Sigma_g^-)$ and $O_2^-(X^2\Pi_g)$. Only the linear encounter complex is slightly stable with a very small positive stabilization energy. The other four structures are very unstable with the negative stabilization energies. However, if using $O_2(^1\Sigma_g^+)$ to react with $O_2^-(X^2\Pi_g)$, the encounter complex with low-spin coupling is favorable from the energy standpoint. The state–state energy separation $E(^1\Sigma_g^+) - E(^3\Sigma_g^-)$ is 30.527 kcal/mol at the MP2 (full)/6-311 + G* level. The calculated stabilization energies are 20.326 (T_1, $^2B_1$), 21.008 (T_2, $^2A_2$), 31.367 (L, $^2A_2$), 20.695 (P, $^2A_2$), and 21.326 (C, $^2A_1$) kcal/mol for this coupling mechanism from $O_2(^1\Sigma_g^+)$ and $O_2^-(X^2\Pi_g)$. Similarly, calculations indicated that the stabilization energies for the high-spin coupling mechanism from $O_2(^3\Sigma_g^-)$ and $O_2^-(X^2\Pi_g)$ are 1.835 (T_1, $^4A_1$), 2.199 (T_2, $^4A_1$), 0.941 (L, $^4A_1$), 2.532 (P, $^4B_2$), and 2.452 (C, $^4A_1$) kcal/mol. Therefore, it appears more probable that the electron transfer in the $O_2 \cdots O_2^-$ system between $O_2(^1\Sigma_g^+)$ and $O_2^-(X^2\Pi_g)$ may take place efficiently via an overall doublet state, while that between $O_2(^3\Sigma_g^-)$ and $O_2^-(X^2\Pi_g)$ may take place efficiently via an overall quartet state. This prediction is in good agreement with the studies on the quartet state coupling mechanism for the $O_2 + O_2^-$ reaction between $O_2(^3\Sigma_g^-)$ and $O_2^-(X^2\Pi_g)$ made by Ohto and Morokuma,[18] Li et al.,[19] and us.[25] This investigation is aimed at the reaction between $O_2(^1\Sigma_g^+)$ and $O_2^-(X^2\Pi_g)$, which may be favorable via a doublet state (low-spin) coupling mechanism. On the other hand, the contact distances are more than 2 times the common O—O bond length and the coupling interaction between two redox species, $O_2(^1\Sigma_g^+)$ and $O_2^-(X^2\Pi_g)$, is weak and the complex structure is floppy. The optimizations for the combined complex $O_2 + O_2^-$ in five geometries are restricted in the doublet state. The optimized five geometries are described in Figure 1; the corresponding energies and other structural properties are summarized in Table II.

The results in Table II indicate that the bond length of one O—O fragment is slightly longer than and close to that of the isolated $O_2(^1\Sigma_g^+)$ molecule, while another O—O fragment has a bond length very close to that of the isolated $O_2^-(X^2\Pi_g)$ molecule. The vibrational frequencies for the two O_2 fragments are also very close to the isolated species $O_2(^1\Sigma_g^+)$ and $O_2^-(X^2\Pi_g)$, respectively. This observation indicates that the excess electron is well localized on the latter O_2 molecular fragment. The net charge populations given in Table II also support this analysis. From the energy standpoint, the more favorable structure is linear (L type, $^2A_2$), because the order in stabilization energy is L ($^2A_2$, 31.367 kcal/mol) > C ($^2A_1$, 21.326 kcal/mol) > T_2 ($^2A_1$, 21.008 kcal/mol) > P ($^2A_2$, 20.695 kcal/mol) > T_1 ($^2A_1$, 20.326 kcal/mol). The T_2-type geometry is given by interchanging the position of O_2^- with that of O_2 and it corresponds to the product geometry of the T_1-type complex. The stabilization energy of the T_1-type structure is 0.7 kcal/mol smaller than that of the T_2-type structure.

For the five encounter complex, the activation barrier heights to the transition state from the corresponding encounter complex $O_2 \cdot O_2^-$ are 2.397 (T_1), 4.056 (T_2), 4.822 (L), 2.774 (P), and 4.635 (C) kcal/mol, respectively. The coupling matrix elements referring to the difference between the activation energy and the energy of the system at the crossing point are 972.6 (T_1), 391.9 (T_2), 123.8 (L), 840.6 (P), and 0.0 (C) cm^{-1} for the five transi-

TABLE II.
Geometrical Parameters, Harmonic Frequencies, Relevant Energies, and Coupling Matrix Elements for Reacting System, $O_2 + O_2^-$, in Encounter Complex and Transition State and Electron Transfer Reaction Rate.

	$T_1(^2B_1)$	$T_2(^2A_2)$	$L(^2A_1)$	$P(^2A_2)$	$C(^2A_1)$
E_d (kcal / mol)			5.175		
Encounter complex					
r(Å)	3.075	2.898	2.975	3.260	3.006
r_0(Å)	1.231	1.229	1.223	1.229	1.228
r_-(Å)	1.357	1.351	1.351	1.357	1.356
E_s (kcal / mol)	20.326	21.008	31.367	20.695	21.326
ω_0 (cm^{-1})	1693.1	1710.6	1704.4	1708.7	1710.4
ω_- (cm^{-1})	1171.4	1169.7	1170.8	1170.9	1175.8
O_2^- net charge	−0.9968	−0.9789	−0.9962	−0.9958	−0.9904
O_2 net charge	−0.0032	−0.0211	−0.0038	−0.0042	−0.0096
Transition state					
$r_0 = r_-$ (Å)	1.292	1.289	1.286	1.291	1.290
E_a (kcal / mol)	2.397	4.056	4.822	2.774	5.175
H_{if} (cm^{-1})	972.6	391.9	123.8	840.6	0.0
$\lvert S_2 - S_1\rvert$ (erg / cm)	12.59	17.67	18.99	13.58	18.65
κ_{el}	0.998	0.647	0.111	0.989	~ 0.0
k_{et}^a ($M^{-1}\,s^{-1}$)	7.014	0.277	0.0131	3.683	~ 0.0
k_{et}^b ($\times 10^{10}\ M^{-1}s^{-1}$)	1.754	0.0694	0.00326	0.921	~ 0.0

[a] In solution.
[b] In a gaseous phase process.

tion states, respectively. The most stable is the T_1-type transition state with C_{2v} symmetry; the coupling matrix element is the largest (972.6 cm^{-1}). This phenomena may be explained in terms of the orbital overlap interaction between the donor and the acceptor (Fig. 2). For T_1-type geometry, only the $\pi_=^*$ of both species (O_2 and O_2^-) is favorable with an effective overlap due to the orbital phase symmetry. This location of the two species not only decreases the nuclear repulsion interaction, but it also increases the orbital overlap between the donor (O_2^-) and the acceptor (O_2); thus, the T_1-type activated state should have a low activation barrier and a large coupling interaction. The *P*-type structure, although the contact distance (3.26 Å) is larger than the other structures, is favorable with both $\pi_=^*$ and $\pi_\perp^*$ overlaps; the coupling matrix element is therefore larger than those of the *C*-type and *L*-type structures and is very close to that of the T_1-type structure with only one $\pi_=^*$ overlap. For the *L*-type structure, although the coupling overlap occurs in both the $\pi_=^*$ and $\pi_\perp^*$ orbitals, only the end O atoms are used for both species (O_2 and O_2^-) to produce the overlap. It may be expected that such a coupling interaction should be small and this linear transition state should have a large activation barrier. The data shown in Table II provide good evidence of this. The *C*-type structure comes from the *P*-type structure by rotating one of two molecular fragments, O_2 or O_2^-, by 90° along the C_2 principle axis. Although the nuclear repulsion interaction decreases and the contact distance becomes small and seemingly favorable with the orbital overlap, the orbital phase symmetry becomes unfavorable: the $\pi_=^*$ overlap changes to zero, as does the $\pi_\perp^*$ orbital coupling. Therefore, the coupling matrix element should be zero and the reacting system

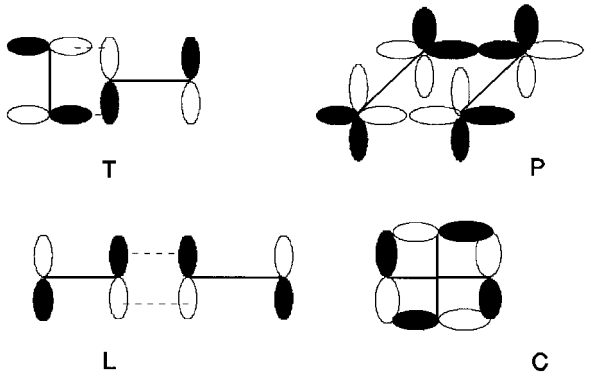

FIGURE 2. The contour of the orbital couplings between the donor and the acceptor.

should have to experience a higher activation barrier during the electron transfer. This analysis may be demonstrated by comparing the activation energies for two structures (5.175 kcal/mol for C, 2.774 kcal/mol for P) and others.

ELECTRON TRANSFER RATE AND EFFECT OF SOLVENT

The electronic transmission coefficient and the transfer rate were calculated in terms of the formulas mentioned above and are listed in Table II. In the calculations the nuclear tunneling factor was estimated as 12, and the used effective collision frequency Z was 10^{12}. The electronic transmission coefficients were calculated in terms of eq. (11) and the corresponding coupling matrix elements and the slopes of the potential energy surfaces. Substitutions of these preexponential factors and the Franck–Condon term in eq. (10) can give the electron transfer rates for the reacting system, $O_2 + O_2^-$, in five different transition states in the gaseous phase process. To estimate the effect of the solvent medium on the electron transfer rate, the solvent correction was also made for the relevant kinetic parameters. Preliminary calculations indicated that the effect of the solvent on the electronic transmission coefficient was small, but that on the activation energy was large. Thus, we only made a correction for the Franck–Condon term. The summation method of the activation energy allowed us to separate it into the inner sphere and the outer sphere contributions and the Franck–Condon term into two parts. For the outer sphere part, an estimate of 23.2 Å^3 was made for the volume of each reactant, which corresponds to a sphere with a radius of 1.8 Å, and E_{out} was estimated from an approximate formula [see eq. (13) in ref. 26] as 12.6 kcal/mol. Therefore, the electron transfer rates in solution may be simply obtained from the corresponding values in the gaseous phase process by multiplying a modifying factor [$\exp(-E_{out}/RT)$]. No experimental value was found for the electron transfer rate for this system in the gaseous process. Many estimated experimental values using the Marcus–Hush cross relation give the result of about 3 mol^{-1} s^{-1}.[24] Our calculated values in the five mechanisms are 7.014 (T_1), 0.277 (T_2), 0.0131 (L), 3.683 (P), and $\sim$ 0.0 (C) mol^{-1} s^{-1}, which are very close to the experimental values. Especially for the T_1-type and the P-type mechanism, good agreement for the electron transfer rate between the experimental and the theoretical values were observed. From this it may be noted that the favorable transition states are the T_1 and the P types. A statistical result within an energy-weighted average gave a value of 1.968 mol^{-1} s^{-1}. In the gaseous process the effect of the solvent medium is a tendency to be zero; the electronic transfer rates become 1.75×10^{10} (T_1), 6.937×10^8 (T_2), 3.264×10^7 (L), 9.212×10^9 (P), and $\sim$ 0.0 (C) mol^{-1} s^{-1}; the statistical averaged value is 4.923×10^9 mol^{-1} s^{-1}. These results are in agreement with the other theoretical value ($\sim 10^8$ mol^{-1} s^{-1})[26]. Calculations of the relevant parameters in the gaseous phase process and in solution also indicated that the coupling matrix elements in the gaseous phase mechanism is very close to those in solution, the effect of the solvent medium on the electronic transmission factor is small, but that on the electron transfer rate is very large, especially for the reactions with low activation barriers.

Conclusions

In conclusion, the electron transfer reactivity of the $O_2 + O_2^-$ system in a low-spin coupling mechanism was studied at the UMP2 (full)/6-311 + G* basis set level for the five selected coupling structures: two T types, collinear, parallel, and crossing. The results indicate that the structures of the encounter complex directly influence the electron transfer reaction mechanism and rate. In general, in structure these kinds of encounter complexes are in a high-spin state and unstable and are not amenable to experimental observation; high quality treatments with electron correlation and large basis sets are needed in theoretical analysis. For this encounter complex involving the negatively charged $O_2 + O_2^-$ coupling system, the contact distances were large, the interaction between the donor and the acceptor was weak, and then the structures were floppy. From the energy standpoint, the favorable electronic states to form low-spin coupling for the two reacting species are $^1\Sigma_g^+(O_2)$ and $X\,^2\Pi_g(O_2^-)$ instead of $X\,^3\Sigma_g^-(O_2)$ and $X\,^2\Pi_g(O_2^-)$. The electron transfer is more likely to take place via the T_1-type and the P-type structures. The electronic transmission factor for this reacting system, $O_2 + O_2^-$ is generally less than unity; thus, the electron transfer reaction is nonadiabatic in nature. In addition, it should be noted that the effect of the solvent molecules on the coupling matrix element is small but that on the electron transfer rate is very large.

References

1. (a) Marcus, R. A. J Chem Phys 1956, 24, 966; (b) Marcus, R. A. J Chem Phys 1965, 43, 679; (c) Marcus, R. A. J Chem Phys 1965, 43, 3477; (d) Marcus, R. A. Faraday Discuss Chem Soc 1982, 74, 7.
2. (a) Hush, N. S. Trans Faraday Soc 1961, 57, 557; (b) Hush, N. S. Electrochim Acta 1968, 13, 1005.
3. Sutin, N. Annu Rev Nucl Soc 1965, 57, 155.
4. Newton, M. D.; Sutin, N. Annu Rev Phys Chem 1984, 35, 437.
5. (a) Newton, M. D. Int J Quantum Chem Quantum Chem Symp 1980, 14, 363; (b) Brunschwing, B. S.; Logan, J.; Newton, M. D.; (c) Sutin, N. J Am Chem Soc 1980, 102, 5978.
6. (a) Brown, G. M.; Sutin, N. J Am Chem Soc 1979, 101, 883; (b) Sutin, N.; Brunschwing, B. ACS Symp Ser 1982, 198, 105; (c) Marcus, R. A. Int J Chem Kinetics 1981, 13, 865; (d) Hupp, J. T.; Weaver, M. J. J Electroanal Chem 1983, 152, 1.
7. (a) Logan, J.; Newton, M. D. J Chem Phys 1983, 78, 4086; (b) Newton, M. D. J Phys Chem 1986, 90, 3734; (c) Newton, M. D. J Phys Chem 1988, 92, 3049.
8. Khan, S. U. M.; Zhou, Z. Y. J Chem Phys 1990, 93, 8808.
9. Bu, Y.; Deng, C. J Phys Chem 1996, 100, 18093.
10. Bu, Y. J Phys Chem 1994, 98, 2290.
11. Bu, Y. J Phys Chem 1995, 99, 11650.
12. Bu, Y. J Mol Struct (Theochem) 1994, 309, 121.
13. Bu, Y.; Song, X.; Deng, C. J Mol Struct (Theochem) 1995, 358, 211.
14. Bu, Y.; Song, X.; Deng, C. Chem Phys Lett 1996, 250, 455.
15. Bu, Y.; Deng, C. J Phys Chem 1997, 101, 1189.
16. Chandrasekher, C. A.; Griffith, K. S.; Gellene, G. I. Int J Quantum Chem 1996, 58, 29.
17. Fahey, D. W.; Bohringer, H.; Fehsenfeld, F. C.; Ferguson, E. E. J Chem Phys 1982, 76, 1799.
18. Ohta, K.; Morokuma, K. J Phys Chem 1987, 91, 401.
19. (a) Li, X.; Tian, A.; He, F.; Yan, G. Chem Phys Lett 1995, 233, 227; (b) Li, X.; Tian, A.; He, F.; Yan, G. Chem J Chin Univ 1995, 16, 775.
20. Lind, J.; Shen, X.; Merenji, G.; Jonsson, B. O. J Am Chem Soc 1989, 111, 7654.
21. (a) Zahir, K.; Espenson, J. H.; Bakac, A. J Am Chem Soc 1988, 110, 5059; (b) Stanbury, D. M.; Mulac, W. A.; Sullivan, J. C.; Taube, H. Inorg Chem 1980, 19, 3735; (c) Stanbury, D. M.; Haas, O.; Taube, H. Inorg Chem 1980, 19, 518; (d) Stanbury, D. M.; Gaswick, D.; Brown, G. M.; Taube, H. Inorg Chem 1983, 22, 1975; (e) Creaser, I. I.; Gene, R. J.; Harrowfield, J. M.; Herlt, A. J.; Sargeson, A. M.; Snow, M. R.; Sprigborg, J. J Am Chem Soc 1982, 104, 6016.
22. Marcus, R. A.; Sutin, N. Biochem Biophys Acta 1985, 811, 265.
23. Frisch, M. J.; Trucks, G. W.; Head–Gordon, M.; Gill, P. M. W.; Wong, M. W.; Foresman, J. B.; Johnson, B. G.; Schlegel, H. B.; Robb, M. A.; Replogle, E. S.; Gomperts, R.; Andres, J. L.; Raghavachari, K.; Binkley, J. S.; Gonzalez, C.; Martin, R. L.; Fox, D. J.; Defrees, D. J.; Baker, J.; Stewart, J. J. P.; Pople, J. A. Gaussian 92, Revision E.1; Gaussian, Inc.: Pittsburgh, PA, 1992.
24. Celotta, R. J.; Bennet, R. A.; Hall, J. L.; Siegel, M. W.; Levins, J. Phys Rev 1972, A6, 631.
25. A comprehensive calculations investigation on $O_2 \cdots O_2^-$ (quartet state, high-spin mechanism): Bu, Y.; Sun, H.; Niu, H. J Mol Struct (Theochem) to appear.
26. Bennett, L. E.; Warlop, P. Inorg Chem 1990, 29, 1975.
27. Huber, K. B.; Herzberg, G. Constants of Diatomic Molecules; Van Nostrand: New York, 1979.